



## Thermally tunable THz filter made of semiconductors

Chuqing Liu, Jiasheng Ye, Yan Zhang\*

Beijing Key Lab for Terahertz Spectroscopy and Imaging, Key Laboratory of Terahertz Optoelectronics, Ministry of Education, Department of Physics, Capital Normal University, Beijing 100048, China

### ARTICLE INFO

#### Article history:

Received 18 May 2009

Received in revised form 6 October 2009

Accepted 9 November 2009

#### Keywords:

Tunable terahertz filter

InSb semiconductor slabs

The finite-difference time domain method

### ABSTRACT

By using the finite-difference time domain method, the transmission properties of terahertz wave passing through two different periodic subwavelength structures on InSb semiconductor slabs under different temperatures have been investigated. The results show that the peak transmittance increases and the transmittance peak has a blue shift when the temperature is increasing. It is extremely versatile to control the tunable THz filter by varying the temperature.

© 2009 Elsevier B.V. All rights reserved.

Terahertz (THz) wavelengths cover the range from 30  $\mu\text{m}$  to 3 mm, sandwiched between the microwave and infrared regions. The THz technology is a rapidly growing research issue in recent years and shows great potential applications in many scientific and technological fields, such as free-space communications, medical and biological imaging, detection of explosives, and spectroscopy [1–4]. With the rapid development of THz radiation sources [5–8] and detectors [9–11], there is also a great demand for THz filters, polarizers, and attenuators [12]. At optical frequencies, Ebbesen et al. discovered the enhanced transmission of light through the array of subwavelength holes perforated on an optically thin metallic film [13]. It has inspired great interest to explore the underlying physics and the possible applications of surface plasmon polaritons (SPP). Most of the researches are related to the SPP in the visible (or near-infrared) domain on metallic surfaces, with the challenge of manipulating the SPP on the nano scale [14]. Recently, similar phenomena have also been found in the microwave and THz wave range [15], which possess great potential applications in the fields of subwavelength optics, optical data storage, and near field microscopy [16].

Except for metals, semiconductors can also support electron plasma oscillations. Semiconductors emulate metals by having the real parts of their relative permittivity negative under adscitious exciting. Besides of this, semiconductors have two significant advantages compared with the metals: (1) their relative permittivity can be modified by changing the temperature, the optical illumination, or the magnetic field. Through changing the carrier

density, the plasma frequency of the semiconductor can be tuned. Therefore, a tunable THz filter can be realized by varying the temperature [17]. (2) The imaginary part of permittivity of metals is quite large in the THz and microwave wavelength ranges, which is harmful for enhancing the light transmission. Fortunately, the permittivity of semiconductors in the THz wave range is similar to that of metals at optical frequencies. It is expected that the semiconductor filter should present a better transmission property than a metallic filter in the THz wavelength region [18].

Since the permittivity of the indium antimonide (InSb) can be easily altered by changing the temperature, we adopt it as the material of the subwavelength structured filter. The transmission properties of the structured slab are investigated by using the finite-difference time domain (FDTD) method. We expect that the transmittance of the THz filter can be controlled by tuning the temperature.

The schematic diagrams of two periodic hole array structures perforated on 20  $\mu\text{m}$  thick InSb slabs are shown in Figs. 1a and b. Fig. 1a presents a InSb slab with 100 ( $x$ -axis)  $\times$  20 ( $y$ -axis)  $\mu\text{m}^2$  rectangular hole arrays, whose periods are 120  $\mu\text{m}$  in two directions. The incident light is along the  $z$ -axis, with the electric field in the  $y$ -axis. Fig. 1b plots the InSb slab with a cruciform hole array, which is composed of the structure shown in Fig. 1a and its rotated structure. In Fig. 1, the white and gray parts represent air and the InSb material, respectively.

When the frequency is smaller than transverse optical phonon frequency, the complex relative permittivity of the InSb material can be given from the simple Drude model as [19]

$$\varepsilon(\omega, T) = \varepsilon(0) - \frac{\omega_p^2}{[\omega^2 + i\gamma(T)\omega]}, \quad (1)$$

\* Corresponding author.

E-mail address: [yizhang@mail.cnu.edu.cn](mailto:yizhang@mail.cnu.edu.cn) (Y. Zhang).

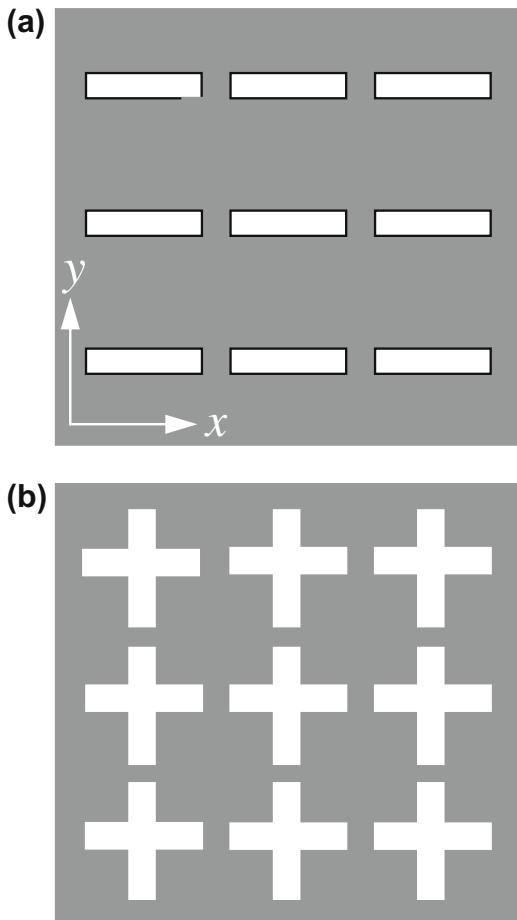


**Fig. 1.** Schematic of two InSb slabs with periodic subwavelength air hole arrays. The white and gray regions represent the air and InSb parts, respectively.

where  $\omega$  is the angular frequency;  $\epsilon(0) = 16.8$  represents the static dielectric constant; the damping constant  $\gamma$  is a function of temperature  $T$ , i.e.,  $\gamma(T)$ . The plasma frequency  $\omega_p = \sqrt{Ne/\epsilon_0 m^*}$  depends on the intrinsic carrier density  $N$ , the electric charge unit  $e$ , the free-space permittivity  $\epsilon_0$  and the effective mass  $m^*$  of free carriers. In contrast to metals, the plasma frequency of the InSb material significantly depends on the temperature  $T$ . The intrinsic carrier density  $N$  (in the unit of  $\text{cm}^{-3}$ ) in the InSb material and the temperature obeys the following relation [20]

$$N = 5.76 \times 10^{14} T^{3/2} \exp(-0.13/k_B T), \quad (2)$$

where  $k_B$  is the Boltzmann constant and the temperature  $T$  is in the unit of Kelvin. A variation in  $N$  due to a variation in  $T$  will lead to a change of  $\omega_p$ . In the terahertz regime,  $\epsilon(\omega)$  of the InSb material is very sensitive to the temperature  $T$ . Consequently, we can expect that temperature variations can cause substantial tunabilities in the responding characteristics of filters.

The influence of the temperature on the transmittance of the InSb slab with rectangular and cruciform hole arrays is plotted in Fig. 2a and b, respectively. For the sake of comparison, the transmittance spectra of the gold slabs with subwavelength air hole arrays are also plotted, whose geometrical parameters are the same as above. In Fig. 2a, two transmittance peaks are observed. One is at 0.23 THz, which is determined by the periodicity of the structure. The other one is obviously enhanced and has a blue shift with the increase of the temperature. It can be explained as follows. According to Eqs. (1) and (2), the permittivity of the InSb material depends on the charge carrier density  $N$  and the damping constant  $\gamma$ , both of which are functions of the temperature. Generally, the

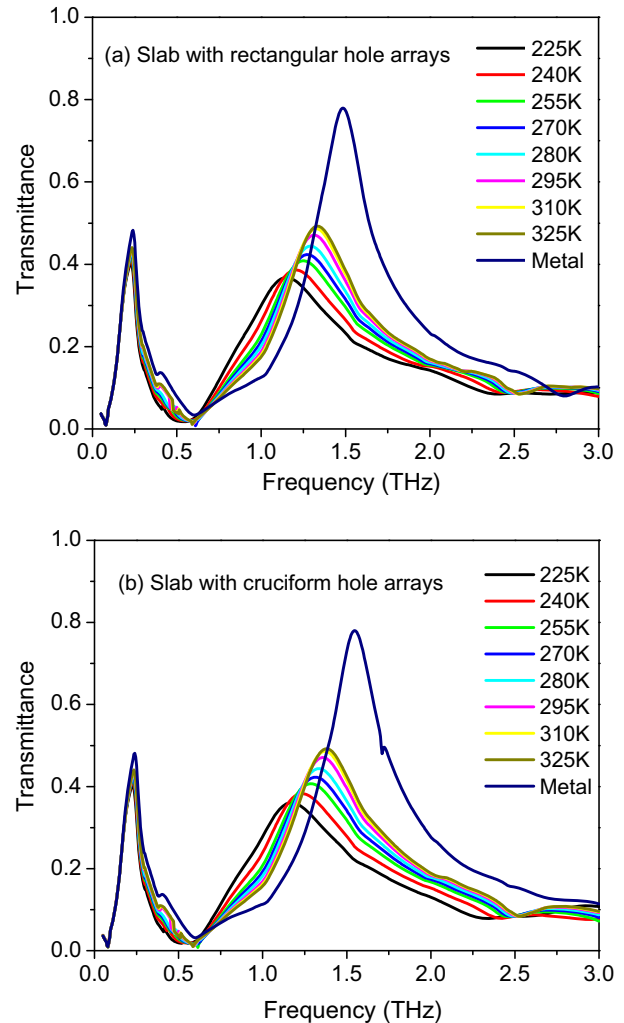


**Fig. 2.** Transmission spectra of the structured InSb slabs at different temperatures ranging from 225 to 325 K. The InSb slab with (a) rectangle hole arrays and (b) cruciform hole arrays. The period is selected as  $120 \mu\text{m}$ .

temperature-dependent resonant characteristics can be mainly attributed to the increase in the density of free carriers by thermal excitation as the temperature increases. For instance, at room temperature, the InSb material has an intrinsic carrier concentration of  $10^{16} \text{cm}^{-3}$ . The electron effective mass in InSb is  $0.015 m_0$ , where  $m_0$  is the electron mass  $m_e = 9.1 \times 10^{-31} \text{kg}$  and  $\epsilon(0) = 16.8$  [19,20]. From Eq. (2), the intrinsic carrier density  $N$  in InSb is about  $2.4 \times 10^{15} \text{cm}^{-3}$  at 225 K; in contrast, it is about  $3.3 \times 10^{16} \text{cm}^{-3}$  at 325 K. It is indicated that the semiconductor InSb displays more metallic features when increasing the temperature. In addition, in Fig. 2a we note that the electric field is along the  $y$ -axis, which is perpendicular to the long side of the rectangular hole in Fig. 1a. Therefore, the electric field acts as TM polarization, and the surface plasmon is easy to be excited on the slab surface. As a result, the transmission is enhanced and the peak position shifts to that of the gold slab (blue shift). Very slight differences are obtained between Fig. 2a and b, which can also be understood. In Fig. 2b, the investigated cruciform hole array structure is composed of two rectangular hole arrays. For the rectangular hole array in the  $y$ -axis, the electric field  $E_y$  behaves like TE polarization, which almost has no contributions to the surface plasmon.

Now let's take an example, for the InSb slab with rectangular hole arrays, to see the surface plasmon phenomena more clearly. The temperature is chosen as 270 K, and the period is  $120 \mu\text{m}$ .

For the second resonant peak at 1.27 THz, the normalized field distribution  $E_z$  on the exit surface of the slab is displayed in Fig. 3. From Fig. 3, it is apparently seen that the electric field resonance is achieved inside the hole arrays and the electric field is attenuated rapidly on the surface as the distance is increased. This surface plasmon effect leads to the peak transmittance.

Fig. 4 shows the frequency dependence of the second resonant peak on the temperature for the two arrays in the range of 225–325 K. The black and blue curves represent the results for the InSb slabs with rectangular and cruciform hole arrays, respectively, whose periods are both 120  $\mu\text{m}$ . It is obviously found that the resonant frequencies increase when the temperature increases. The gradually increasing frequencies approach to the saturation values of 1.49 THz and 1.55 THz for rectangle and cruciform hole arrays respectively, which are resonant frequencies of the gold structured slabs with the same parameters, as shown by the black and blue dashed lines in Fig. 4. Therefore, the resonant frequency of the filter can be tuned by controlling the temperature.

Moreover, changing the period of the structure, we calculate the peak transmittance and the second resonant frequency of the two

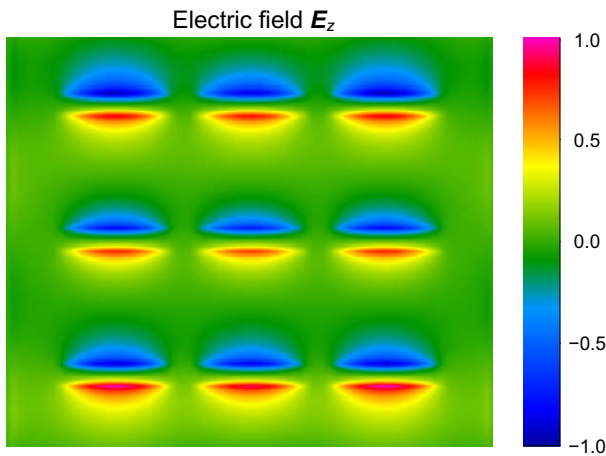


Fig. 3. For the second resonant frequency of 1.27 THz in Fig. 2a, at the temperature of 270 K, the electric field distribution  $E_z$  on the exit surface of the InSb slab with rectangular hole arrays, whose period is 120  $\mu\text{m}$ .

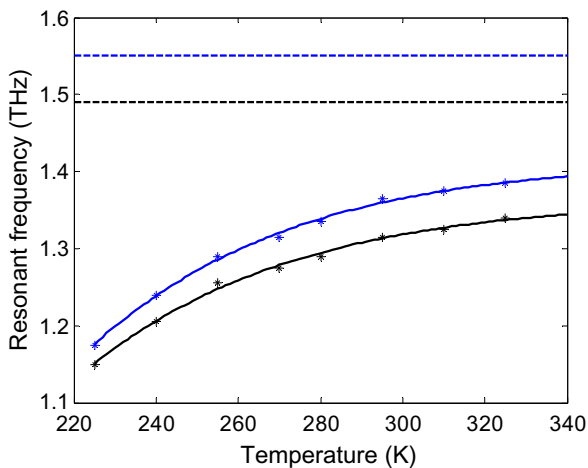


Fig. 4. Dependence of the resonant frequency  $\omega$  on the temperature  $T$ . The black and blue curves represent the results for the InSb slabs with rectangular and cruciform hole arrays, respectively, whose periods are both 120  $\mu\text{m}$ . The black and blue dashed lines indicate the results for the corresponding gold slabs with the same parameters. (For interpretation of the references to colour in this figure legend, the reader is referred to the web version of this article.)

structured InSb slabs at the temperature of 270 K, as seen in Fig. 5. The blue curves with square markers and with crisscross markers represent transmittance of slabs with rectangular and cruciform hole arrays, respectively. The black curves with square markers and with crisscross markers represent the corresponding resonant frequencies. It is obviously demonstrated that both the peak transmittance and the resonant frequency are decreased as the period is increased. Compared with the InSb slab with rectangular hole arrays, the InSb slab with cruciform hole arrays has a larger resonant frequency and a smaller peak transmittance.

The variation of  $\epsilon(\omega)$  with respect to the temperature  $T$  is shown in Fig. 6. The real and imaginary parts of  $\epsilon(\omega)$  are illustrated by the solid and dashed curves, respectively. The black, blue, red, and magenta colors represent different temperatures of 225, 255, 280, and 325 K, respectively. As the temperature increases, the real part of the  $\epsilon(\omega)$  drops rapidly, while the imaginary part increases. Clearly, the InSb material exhibits dielectric or metallic features at low or high temperatures, respectively.

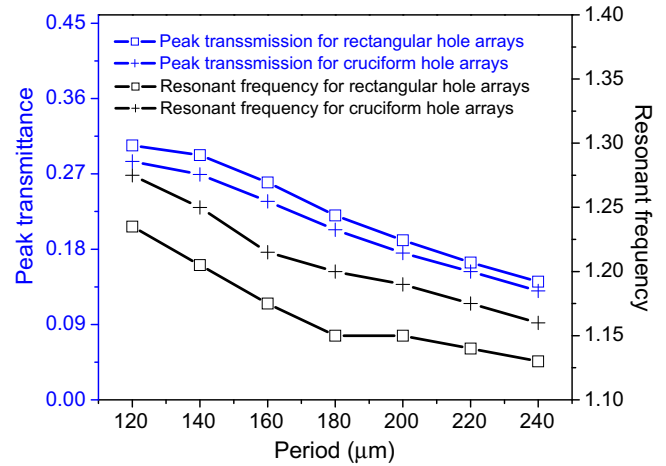


Fig. 5. The transmittance and the resonant frequency of the second peak for the InSb slabs with hole arrays versus the period of the structure. The temperature is selected as 270 K.

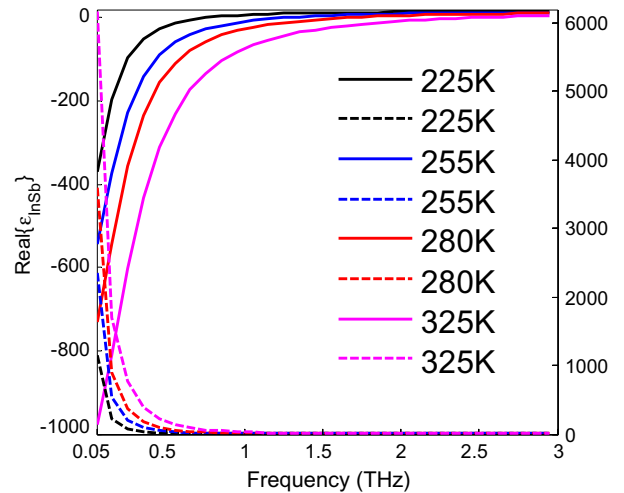


Fig. 6. The real (solid curve) and imaginary (dashed curve) parts of the relative permittivity of the InSb material at different temperatures. The black, blue, red, and magenta curves indicate different temperatures of 225, 255, 280, and 325 K, respectively. (For interpretation of the references to colour in this figure legend, the reader is referred to the web version of this article.)

In conclusion, the transmittance properties of the InSb slabs with periodic subwavelength hole arrays under different temperatures are theoretically investigated by using the FDTD method. It shows that the resonant transmittance increases and the resonant frequency has a blue shift as the temperature is increasing. It provides a versatile way to tune the THz filter under thermal excitation.

### Acknowledgements

This work was supported by the National Basic Research Program of China (Grant Nos. 2006CB302901 and 2007CB310408), the National Natural Science Foundation of China (NNSFC) (Grant Nos. 10604042 and 10674038), and the Funding Project for Academic Human Resources Development in Institutions of Higher Learning under the Jurisdiction of Beijing Municipality.

### References

- [1] J.Z. Xu, X.C. Zhang, *Appl. Phys. Lett.* 88 (2006) 151107.
- [2] H. Zhong, A.R. Sanchez, X.C. Zhang, *Opt. Express* 14 (2006) 9130.
- [3] J.F. Federici, B. Schulkin, F. Huang, D. Gary, R. Barat, F. Oliveira, D. Zimdars, *Semicond. Sci. Technol.* 20 (2005) 266.
- [4] H.B. Liu, G. Plopper, S. Earley, Y. Chen, B. Ferguson, X.C. Zhang, *Biosens. Bioelectron.* 22 (2007) 1075.
- [5] R. Kohler, A. Tredicucci, F. Beltram, H.E. Beere, E.H. Linfield, A.G. Davies, D.A. Ritchie, R.C. Iotti, F. Rossi, *Nature* 417 (2002) 156.
- [6] J.C. Cao, X.L. Lei, A.Z. Li, H.C. Liu, *Appl. Phys. Lett.* 78 (2001) 2524.
- [7] J.C. Cao, H.C. Liu, X.L. Lei, *J. Appl. Phys.* 87 (2000) 2867.
- [8] H.C. Liu, M. Wachter, D. Ban, Z.R. Wasilewski, M. Buchanan, G.C. Aers, J.C. Cao, F.S. Feng, B.S. Williams, Q. Hu, *Appl. Phys. Lett.* 87 (2005) 141102.
- [9] H.C. Liu, C.Y. Song, A.J. Spring Thorpe, J.C. Cao, *Appl. Phys. Lett.* 84 (2004) 4068.
- [10] J.C. Cao, *Phys. Rev. Lett.* 91 (2003) 237401.
- [11] S.W. Gao, J.C. Cao, S.L. Feng, *Commun. Theor. Phys.* 39 (2003) 327.
- [12] D. Wu, N. Fang, C. Sun, X. Zhang, W.J. Padilla, D.N. Basov, D.R. Smith, S. Schultz, *Appl. Phys. Lett.* 83 (2003) 201.
- [13] T. Ebbesen, H. Lezec, H. Ghaemi, T. Thio, P. Wolff, *Nature* 391 (1998) 667.
- [14] A.V. Zayats, I.I. Smolyaninov, A.A. Maradudin, *Phys. Rep.* 408 (2005) 131.
- [15] Q. Xing, S. Li, Z. Tian, D. Liang, N. Zhang, L. Lang, L. Chai, Q. Wang, *Appl. Phys. Lett.* 89 (2006) 041107.
- [16] W.L. Barnes, A. Dereux, T.W. Ebbesen, *Nature* 391 (2003) 824.
- [17] J.A.S. Gil, J.G. Rivas, *Phys. Rev. B* 73 (2006) 205410.
- [18] H.J. Lezec, A. Degiron, E. Devaux, R.A. Linke, L.M. Moreno, F.J.G. Vidal, T.W. Ebbesen, *Science* 297 (2002) 820.
- [19] B. Gelmont, R. Parthasarathy, *Semiconductors* 42 (8) (2008) 924.
- [20] P. Halevi, F.R. Mendieta, *Phys. Rev. Lett.* 85 (2000) 1875.